Geometric and hardness characterization of additively manufactured copper using bound powder extrusion with thermal sintering

Roy Urwin[1] *& Bradley D.* Bock[1*]

[1]Clean Energy Research Group, Department of Mechanical and Aeronautical Engineering, University of Pretoria, South Africa

Abstract. Recent advancements now allow for high thermal conductivity metals such as copper to be additively manufactured and will allow for the applications of the technology to be broadened in the field of heat transfer. In this study, copper samples were additively manufactured using a bound powder extrusion process and then characterised in terms of hardness, porosity, mass, volume shrinkage and surface roughness. It was found that this additively manufactured material has a significantly reduced hardness when compared to pure copper and a porosity of between 32-38%. During the manufacturing process a mass loss of up to 8% and a volume loss of up to 28% was seen compared to the original printed part. The surface roughness (R_a) on the sides of the sample was 14 µm while the tops and bottoms of the sample had a surface roughness 8 µm, both significantly higher than parts produced with traditional machining processes. Designers of heat exchangers that makes use of bound powder extrusion will thus have to compensate for geometry changes between the initial print and final part as well as reduced hardness (and likely strength). Greater porosity and roughness of their parts will also have to be considered, which in some cases like boiling can be an advantage, while in convective heat transfer may be disadvantage.

1. Introduction

Recent advancements in the additive manufacturing field now allow for high thermal conductivity metals to be manufactured with relative ease. This poses an interesting opportunity for the heat transfer industry. Additive manufacturing generally allows for the creation of more complex geometries than commercial subtractive manufacturing allows [1]. This allows for the opportunity to create complex and intricate structures that are optimized for heat transfer that in the past could only exist in theory. The properties however of parts produced through additive manufacturing are different to traditionally manufactured parts. For example, additive manufactured parts generally produce parts with an increased surface roughness [2], which will need to be factored into designs. In some fields, such as pool boiling, increased surface roughness is typically a positive, as it increases the number of nucleation sites present on a given material and thus enhances the pool boiling heat transfer coefficient [3]. In applications where flow is present, such as convective heat transfer, the

* Corresponding author: bradley.bock@up.ac.za

increased roughness will increase pressure drop and thus operational losses [4], a factor that design engineers need to consider.

The different additive manufacturing methods are a further influence on these properties. Metals are typically additively manufactured by spreading a fine layer of metal powder over a surface and then using a laser to selectively melt the powder, fusing the metal together and creating the component [1]. The issue that arises when using copper in this process is that due to the extremely high thermal conductivity of copper, the heat from the laser is dissipated throughout the entire metal powder layer, preventing a component from being printed [5].

To overcome this manufacturers are using a technology known as wax casting [6]. This method 3D prints a mold out of wax for the part. After which the mold is then used in a lost wax casting procedure to create the part [6]. Another method by which these components can be 3D printed is a 3D printing technique known as jet binding, which applies a layer of metal powder to a surface after which a binding polymer is applied to the layer allow to hold the metal powder together [7]. This process is repeated until the part is printed finally the part is sintered to create a fully metal part [7].

A technology gaining traction for the printing of high thermal conductivity metals is Bound Powder Extrusion (BPE) [7], also known as *Metal Filament Extrusion*, *3D Metal Extrusion* or trademarked as *Bound Metal Deposition* by Desktop Metal [8]. This procedure uses a specialized filament that mixes polylactic acid (PLA) plastic and metal powder. This filament is then used to print components in the same way as the classic Fused Filament Fabrication (FFF) processes used for plastic, but after which the part is then debound and sintered, which respectively removes the plastic and fuses the metal powder, thus creating the solid metal component [9]. The plastic is removed typically either through heat or by chemical means, while the metal is typically fused through thermal sintering. This method allows for high thermal conductivity metals to be additively manufactured without encountering the issue seen in other methods.

Studies on the properties of BPE printed copper parts with thermal sintering are scarce. Studies by Bock et al. [10] and Ebrahimi and Ju [11] confirm that BPE technique produces parts with properties differing significantly from the base material. Two key differences were identified: porosity of the final component and heat treatment from the debinding time and sintering time. Montes-Ramirez et al. [12] performed research on copper parts printed with BPE and noted the importance of preventing impurities from entering the part during printing process, but they did not attempt to measure any properties.

Ultrasonic-assisted pressureless sintering (UAPS) of parts produced by BPE was investigated by Singh and Pandey [13], who reported a thermal conductivity for additively manufactured copper to be approximately 280 W/mK with surface porosity of 6.8%. Singh and Pandey [13] also performed tensile tests and obtained an Ultimate Tensile Strength of between 7.67-62.83 MPA with the Ultimate Tensile Strength being a function of sintering temperature and length.

Looking to other additive manufacturing methods of metals, studies on the properties of parts produced with laser-based additive manufacturing methods show significant differences between these parts and traditional methods, and the importance of these differences. Wang et al. [14] noted that increased porosity reduced the thermal conductivity, electrical conductivity, fatigue performance and hardness of the material.

Binder jet printing studies by Thang Q. Tran, et al. [15] found that copper components attained a density of between 76 and 86 % of the density of pure copper, whereas Constantina,

et al. [16] achieved a density of 95 % and a volume shrinkage of between 35 and 45%. Additionally, Constantina, et al. [16] tested the surface roughness of their parts and found a surface roughness (R_a) of 18 µm while successfully additively manufacturing heat sinks of complex geometry using binder jet printing.

This paper seeks to expand the information on the resulting properties of BPE parts produced with thermal sintering, given the lack of literature that focusses on it. Some properties relevant to heat transfer designers will be focussed on, namely porosity, volume and mass reduction and surface roughness, while hardness will be characterized as a simple predictor of strength of the final parts.

2. Methodology

2.1. Additive manufacturing process

2.1.1. Printing process

The samples were printed using a FFF style 3D printer, where filament composed of copper powder and a polymer matrix was extruded to produce the part. An Ender 5 Plus 3D printer was used to print the samples, with the only modification to the printer being that the nozzle of the printer was change from a brass 0.4 mm nozzle to a hardened steel 0.6 mm nozzle as per filament manufacturer's (The Virtual Foundry) recommendation [17]. Additionally, the filament was passed through a "filawarmer" which preheated the filament before entering the printer. This was done to make the filament more flexible and prevent filament breakage [18]. The filament was printed with a nozzle temperature of 235 °C, bed temperature of 60 °C and a print speed of 60 mm/s [17].

2.1.2. Debinding and sintering

The following process was followed to debind and sinter the 3D printed samples.

The debinding process.

The crucible was filled to the halfway mark with refractory (aluminum oxide (AlO_3)) and compacted into the crucible. Then the part was placed into the crucible and covered in refractory and compacted again. Finally, the crucible was placed into the kiln and debound using The Virtual Foundry's method [19].

- Heat the kiln to 482°C at a rate of 56°C per hour.
- Keep the kiln at the temperature for 4 hours.
- Allow the kiln and the part to cool to room temperature.

After which the part was removed from the crucible and the refractory salvaged for later use.

The sintering process.

For sintering the same process for preparing the sample is used as in the debinding process. However, in this case the refractory is Talc powder.

As an additional step to the sintering process The Virtual Foundry recommends that the user cover the top of the crucible in sintering carbon [20].

The reason that sintering carbon is applied is to prevent oxidation from occurring during the sintering process [20]. Due to the high temperature of the sintering process the risk of oxidation is extremely high and if oxidation were to occur it could possibly ruin the part rendering it unless. Finally, the crucible was placed into the kiln and sintered using The Virtual Foundry's method [19].

- Heat the kiln to a temperature of 1052°C at a rate of 111 °C per hour.
- Hold this temperature for 5 hours.

Post sintering cooling.

After the sintering process is complete, the part is cooled. How this is done will influence is the final material properties, and thus serves as an effective heat treatment process.

In this study, after sintering, the part was left in the kiln and both were allowed to cool to room temperature, after which the part was removed from the crucible.

2.1.3. Copper filament used

The filament was composed of 90% copper powder and 10% polymer matrix by weight [17], with a density of between 4500-4700 kg/m^3. Since the density of copper is approximately 8940 kg/m^3 [21] and PLA be 1240 kg/m^3 [22], this means a volume fraction of PLA of only around 37%.

2.2. Samples

In this research 10 mm cubes were 3D printed with the copper filament and then taken through the debinding and sintering process. An example of the cubes used is shown in Fig 1 with the cube on the left being a sintered one and the cube on the right being presintered, additionally, a reference sample machined from C110 was also tested as a control and validation step for testing.

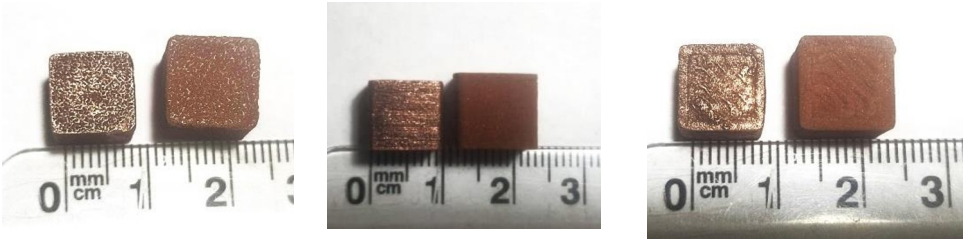

(a) **(b)** **(c)**

Fig 1: Showing a bottom (a), side (b) and top (c) of a sintered and presintered part used in this study.

2.3. Porosity

The porosity (ϕ) of the samples can be determined using the following formula.

$$\phi = \frac{V_{void}}{V_{Total}} \times 100 \quad (1)$$

Where V_{void} was equal to the volume occupied by empty space found within the sample and V_{Total} was equal to the total volume of the sample inclusive of voids and material ($V_{material}$).

Often this is practically measured as follows.

$$\phi = \frac{V_{Total} - V_{material}}{V_{Total}} \times 100$$

Practically, determining V_{void} or $V_{material}$ directly was challenging, therefore with some manipulation the porosity equation is converted to the form shown in Equation 2 below.

$$\phi = 1 - \frac{m_{ps}}{\rho_{ref} V_{Total}} \times 100 \quad (2)$$

Where ρ_{ref} was the density of the pure non porous copper (value of 8940 kg/m^3) [17, 21]. m_{ps} was the mass of the sintered sample in kilograms (kg) and V_{Total} was the same value as seen in Equation 1.

Please note that V_{Total} is the total volume of the sample after sintering and has an error of 0.3 mm^3. This combined with Equation 2 and the uncertainty of the mass (0.01 g) was used to calculate the uncertainty using the "Law of the propagation of uncertainty" [23] shown in Equation 3 to determine the uncertainty of Equation 2. The uncertainty of the porosity was determined to be less than 5%.

$$\Delta y^2 = \sum_{i=1}^{N} \left(\frac{dy}{dx_i}\right)^2 \Delta x_i^2 \quad (3)$$

Where Δy is the uncertainty of the function for which the uncertainty is needed, $\frac{dy}{dx_i}$ is the partial derivative of the function y with respect to variable x_i and Δx_i is the uncertainty associated with variable x_i.

2.4. Hardness

The Vickers hardness measurements were conducted on a Struers Duramin 40 M1 hardness tester (error 0.25% [24]) where a diamond tipped point was pressed into the sample with a force of 1 kg and a hold time of 10 seconds after which the dimensions of the indentation were measured by microscopic inspection using the tester. This was then repeated three times for each sample evaluated at different points along the sample's length.

2.5. Volume and mass reduction

The volume and mass reduction during sintering were calculated using the mass and the overall dimensions of the sample. The mass of the sample was obtained using a ADAM HCB 1002 digital scale (error of 0.01 g) and the overall dimensions using a vernier calliper (error of 0.02 mm). During the debinding stage some of the samples became distorted due to expanding gas inside the sample. In such cases an average of the overall dimensions were taken using multiple measurements across the sample.

The uncertainty of the mass measurements was approximately 0.25% of these samples mass and the volume was approximately 0.03 %. The density of the sample was also calculated to have an uncertainty of approximately 0.22%.

2.6. Surface roughness

The average surface roughness (R_a) in micrometres was measure using a diamond tipped profilometer (Mitutoyo SJ-210). This tester taps the surface of the samples with a diamond tip, measuring the displacement of the of the tip to obtain the surface roughness with a maximum error of 0.02 µm [25]. The top, bottom and one side of each sample were tested three times and then averaged to obtain the results within this report.

3. Results

3.1. Volume and mass reduction

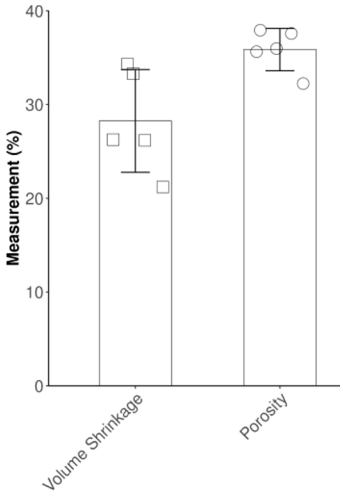

Fig 2: Volume shrinkage and porosity measurements.

It was found that on a volume basis the sintering process reduces the volume of the given sample by an average of 28 % across five samples, which was expected since the volume percentage of PLA in the filament is around 37 %. However, as can be seen in Fig 2 there is spread in the data and a value as high as 35% or as low as 22% was measured in this study.

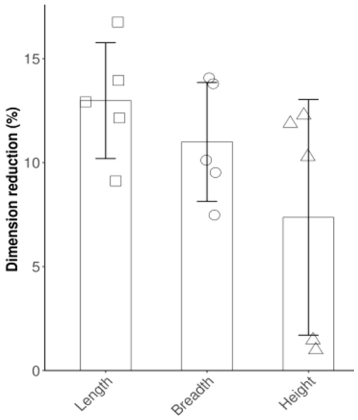

Fig 3: Showing the result of the dimensional shrinkage.

If one considers the dimension specific shrinkage (i.e., the change in length, breadth and height of the sample during sintering), it was found that each dimension reduces roughly by 12 %, with some outliers on the height shrinkage, as seen in Fig 3. If the outliers on the height shrinkage are ignored, the volume shrinkage relatively uniform across the samples. This contradicts previous findings that there is generally more shrinkage in the vertical direction due to the effects of gravity [26]. Considering the small size of these samples, it is likely that the weight effect was not significant enough to affect the results.

The two outliers in Fig 3 show that majority of the shrinkage occurred in the length and very little shrinkage occurred in the height. While it is possible that these samples are simply outliners from the norm, a possible explanation for this is that they had an uneven distribution of PLA and copper throughout the sample resulting in uneven shrinkage. Another possible cause is that during the sintering process either due to part orientation or air pockets in the refractory the length saw more heat than the other dimensions and the height shrinkage was reduced as a result.

In terms of mass reduction, it was found that the mass reduction during sintering was between 8 and 9 %., which aligns with the fact that the mass of PLA present in the filament was between 10-13 % [27]. Due to the volume reduction being significantly higher than the reduction in mass this has resulted in a significant increase to the samples' density during sintering. Before sintering the density of the samples tested were approximately 4 500 kg/m^3 and after sintering the density of the sample increased to approximately 5 500 kg/m^3. Since the sintering process removes the PLA from the sample, the increase in density is expected, as the PLA occupies a large proportion of the volume while occupying a small proportion of the mass.

3.2. Porosity

The samples sintered in this study had an average porosity of 35 %, with a range from 32 to 38 %, as shown in Fig 2. This value stands in contrast to the study conducted by Bock et al. [10] that documented a porosity lying between 20 and 27 %. Ebrahimi and Ju [11] reported a porosity as high as 55% in the samples that they tested. From comparing these three values there is a very large variation that can occur in the porosity of the samples.

The large difference between sample porosity could be due to the sintering process. Ebrahimi and Ju [11] followed a similar initial process used in this study, however the sintering process was changed, with a debinding temperature of 350 °C and a hold time of 3 hours, while the sintering temperature was 980 °C with the sintering hold time was 50 minutes, compared to 1052°C sintering temperature used in this study. This is likely why Ebrahimi and Ju [11] achieved a porosity of 55% as a reduced sintering temperature would result in the removal of the PLA but the part would not reach a temperature high enough to cause the metal to further fuse together likely leaving large pores in the final part. Ebrahimi and Ju [11] then raised the sintering temperature to 1080 °C in order to improve thermal properties and found the porosity dropped to 38 %, with thermal conductivity roughly doubling. Bock et al. [10], Montes-Ramirez et al. [12] and this paper used the original sintering temperature recommended by the Virtual Foundry of 1052°C.

Bock et al. [10] and this study showed that a porosity of 20 – 35 % is a more realistic estimate of the sintered parts if the standard process is followed. Montes-Ramirez et al. [12] on the other hand obtained porosity values of approximately 14% which is much lower than other findings. However Montes-Ramirez et al. [12] obtained their porosity values by microscope inspection. As will discussed later in this report, based on visual inspection, the porosity distribution across the printed sample is not uniform. Thus, microscope inspection may not return the most accurate porosity values depend on how the inspection was carried out. Additionally, based on Bock et al. [10] and this study a variation of 15 % is still quite large from an experimental point of view. Therefore, more research should be done to correlate the porosity more accurately and refine the process to reduce variability.

Fig 4: A cross-section of a successfully debound and sintered part.

To investigate the nature of the porosity distribution, a rectangular sample was printed and sintered, cut into strips and polished, with the resulting information shown in Fig 4. It was found that the pore size is not uniform across the samples with some regions of the sample having extremely large pores and other regions having next to none.

A possible cause for the uneven porosity is that air pockets were trapped in the part during the printing process, as the pores appear to be aligned with the layer lines. This air would then expand during the debinding and sintering process displacing material and causing the pores, separating subsequent layers from each other. Additionally, in the debinding process the PLA binder is turned to gas and sublimates out of the part. It is also likely that this gas becomes trapped in the part and causing pores to form as the gas expands. This possible

explanation seems the most likely as it was noted visually during the study that the majority of the deformation and likely pore formation in the part occurred during the debinding stage.

3.3. Hardness

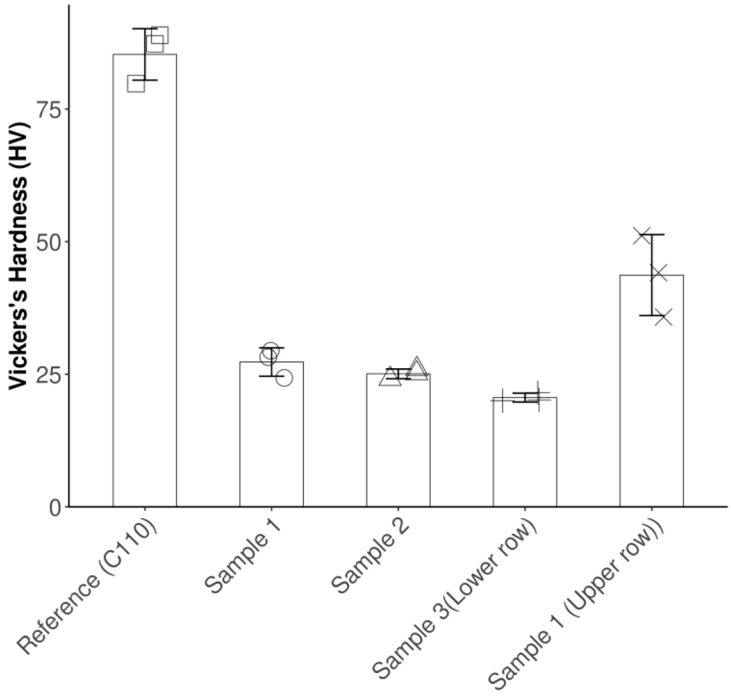

Fig 5: Vickers hardness tests results.

Vickers hardness values are shown in Fig 5. The sintering and post sintering cooling process significantly reduces the hardness of the material, with the samples being tested in this paper having an average hardness value of 25 HV for three samples tested, approximately half of what The Virtual Foundry [27] and Bock et al. [10] found the hardness to be which was approximately a value of 50 HV.

A possible explanation as to why the hardness value seen in this study is significantly lower than expected is due to the increased porosity seen in the samples reducing the hardness. Additionally, The Virtual Foundry [27] and Bock et al. [10] may have used a different cooling process once sintering is complete than in this study, which would serve as a heat treatment process.

Wang et al. [14] while not stating exact values makes note that the hardness of a additively manufactured part is reduced when compare to a part that has been conventionally manufactured which helps validate the finding.

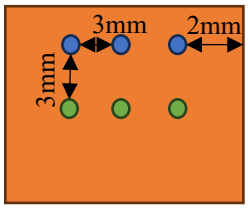

Fig 6: Showing an illustration of the test locations for the sample that was retested.

To confirm the measurements in Fig 5, sample 3 was subjected to the hardness testing again however in a different location as shown in Fig 6. With the location of the orginal measurments shown with blue (Upper row) and the second measurements shown in green (Lower row) for both Fig 6 and Fig 7. Please note that both tests were included in Fig 5

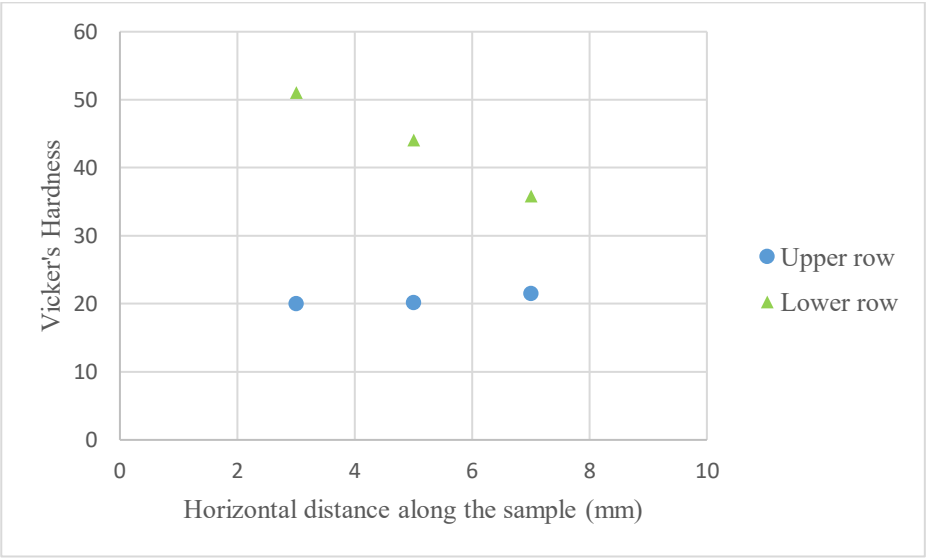

Fig 7: Showing the results of hardness testing across a single sample at different locations.

The results of this test are shown in Fig 7, with an average overall hardness of 32 HV was obtained for the entire sample. However, the hardness values obtained from the second test are more in line with the values found in literature, which is higher than the values obtained across all the other samples. This possibly implies that the hardness of the material is higher towards the center of the sample. Referring to Fig 4 a possible explanation for the inconsistent hardness values is due to the inconsistently in the pore distribution. From Fig 7 it appears that the hardness of the sample follows a linear trend along the sample's horizontal axis. A possible explanation for this is that the internal pore distribution is causing this linear trend however since only one sample was tested significantly more testing is required to confirm this.

This lower hardness the BPE produces is an indicator that the strength of the part is likely reduced, which design engineers using this method would have to consider in their designs.

3.4. Surface roughness

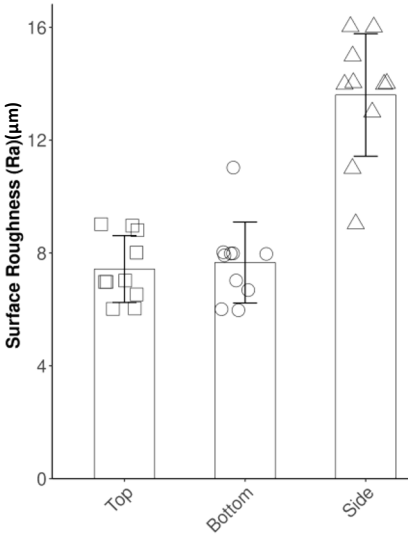

Fig 8: Surface roughness (R_a) test results.

Six samples were subjected to surface roughness tests where the top, bottom and one side of the samples were tested. Note that 2-3 measurements were taken for each surface of every sample so that the consistency of the surface roughness could be assessed. As can be seen in Fig 8 the sintered samples have a surface roughness 3-4 times that of a standard surface for either milling or turning (approximately 3.2 µm) [28].

It was found that the surface roughness does not vary drastically across the top and bottom surface, with the top and bottom surface both having a surface roughness of around 8 µm. As shown Fig 8 the sides of the samples have the highest surface roughness with an average value of approximately 14 µm. Additionally, it appears that the surface roughness of the sides of the sample have a larger spread.

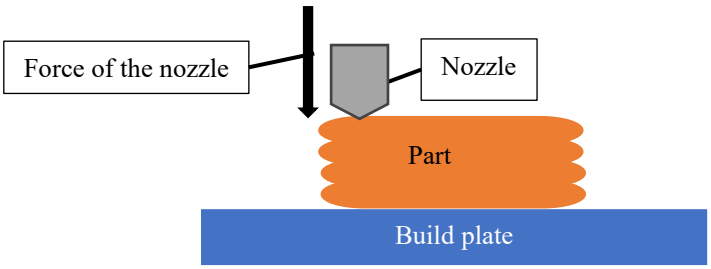

Figure 9: Showing surface roughness forms during printing.

The reason is surface roughness of the bottom surface is lower than the other areas is that the build plate prevented imperfection form developing during the printing process, while the reason the top surface has a low surface roughness was the nozzle pressing down (illustrated in Figure 9) on the surface causing it to be smoother. The sides of the sample have the highest

surface roughness likely due to the layer lines that from during printing causing the surface to be more uneven as shown in Figure 9

It seems apparent that the surface roughness of the additively manufactured parts is dominated by the method in which the material is laid by the nozzle, rather than the sintering process. Overall, even the smoothest section is rougher than a part produced through lathing or milling. Considering that surface roughness is known to increase boiling heat transfer, this suggests heat transfer parts that are additively manufactured will be well suited to this application [29], while flow applications will suffer from the increased pressure drop (and operational costs) due to the increased friction factor as a result of increased roughness.

4. Conclusion

In terms of mass reduction, it was found that the mass appears to reduce consistently at approximately 8 % during the sintering process, while in terms of volume reduction, the sintering process reduces the volume significantly by approximately 28 %. Fortunately, this volume reduction is uniform across a sample of regular geometry if the parts are relatively small (~10 cm). However, there was large variation in some parts, suggesting that if the BPE process is not tightly controlled, large variations can occur. The density of the sample increased from 4500 kg/m^3 to approximately 5500 kg/m^3.

The porosity of sintered additively manufactured copper using BPE varies between 32 to 38 % in this study. These results do not align with the wide range of reported porosities in the limited literature that is available, which suggests that despite using nominally the same manufacturing methods, porosity can still be heavily influenced by changes in process.

The hardness testing showed that the sintering process significantly reduces the hardness of the copper being used. Literature states that the hardness of the material is reduced from a value of 90 HV [10] to a value of 50 HV. However, from this study it was found that the hardness value can be as low as 25 HV. It seems apparent that the hardness is not consistent throughout the material and the hardness was higher 50 HV towards the center of the sample. The reason for this is likely due to the inconsistency in pore sizes throughout the sintered material or heat treatment as a result of cooling time after sintering.

In terms of surface roughness one can expect an overall roughness (R_a) 14 µm on the sides of the part, while the bottom and top surface of the sample can have a surface roughness of 8 µm can be expected. It seems that the surface finish is more dependent on the printing process than the sintering process.

Designers of heat exchangers that makes use of bound powder extrusion will thus have to compensate for geometry changes between the initial print and final part as well as reduced hardness (and likely strength). Compensation for greater porosity and roughness of their parts will also have to be considered, which in some cases like boiling can be an advantage, while in convective heat transfer may be disadvantage due to increased pressure drop.

References

1. HUBS. *What is metal 3D printing and how does it work?* 2023 [cited 2023 21 March]; Available from: https://www.hubs.com/knowledge-base/introduction-metal-3d-printing/.

2. Tamás Markovits and L.F. Varga, *Investigating the surface roughness of 3D printed metal parts in case of thin 20 µm build layer thickness.* Journal of Materials Research 2024. **39**: p. 10.
3. Rohsenow, W.M., J.P. Hartnett, and Y.I. Ch, *Handbook of heat transfer*. 3 ed. 1998, New York: McGraw-Hill.
4. Cengel, Y. and A. Ghajar, *Heat and Mass Transfer: Fundamentals and Applications*. 6 ed. 2020: McGraw Hill.
5. The Editors of Encyclopædia Britannica. *Bronze*. 2024 [cited 2024 18 Feburary]; Available from: https://www.britannica.com/technology/bronze-alloy.
6. Materialise. *Bronze*. n.d. [cited 2024 18 February]; Available from: https://i.materialise.com/en/3d-printing-materials/bronze.
7. Markforged. *Types of 3D Printing in Metal*. n.d. [cited 2024 25 March]; Available from: https://markforged.com/resources/learn/design-for-additive-manufacturing-metals/metal-additive-manufacturing-introduction/types-of-3d-printing-metal.
8. Desktop Metal. *Deep Dive: Bound Metal Deposition (BMD)*. 2022 [cited 2024 26 March]; Available from: https://www.desktopmetal.com/resources/deep-dive-bmd.
9. The Virtual Foundry. *Getting Your Own Custom 3D Printing Filament*. 2022 [cited 2023 21 March]; Available from: https://thevirtualfoundry.com/wp-content/uploads/2022/01/Getting_Your_Own_Custom_3D_Printing_Filament.pdf.
10. Bock, B.D., K. Pretorius, and S. Scott. *3D printing for heat transfer: characterisation of additive manufactured copper*. 2023 [cited 2024 18 Feburary]; Available from: https://www.matec-conferences.org/articles/matecconf/abs/2023/15/matecconf_rapdasa2023_08004/matecconf_rapdasa2023_08004.html.
11. Ebrahimi, N.D. and Y.S. Ju. *Thermal conductivity of sintered copper samples prepared using 3D printing-compatible polymer composite filaments*. 2018 [cited 2024 16 February]; Available from: https://www.sciencedirect.com/science/article/pii/S221486041830575X.
12. Montes-Ramirez, J.E., et al., *Shrinkage and deformation compensation in metal fused filament fabrication (mf3) sintered copper components using 3d scanning and inverse deformation.* Journal of Manufacturing Processes, 2024. **121**: p. 10.
13. Gurminder Singh and P.M. Pandey. *Experimental investigations into mechanical and thermal properties of rapid manufactured copper parts*. 2019 [cited 2024 20 September]; Available from: https://www.researchgate.net/publication/335881134_Experimental_investigations_into_mechanical_and_thermal_properties_of_rapid_manufactured_copper_parts.
14. Wang, S., et al., *Role of porosity defects in metal 3D printing: Formation mechanisms, impacts on properties and mitigation strategies.* Material Today, 2022. **59**: p. 27.
15. Thang Q. Tran, et al. *3D Printing of Highly Pure Copper*. 2019 [cited 2024 20 September]; Available from: https://www.mdpi.com/2075-4701/9/7/756.
16. Loic Constantina, et al. *Laser 3D printing of complex copper structures*. 2020 [cited 2024 20 September]; Available from: https://www.sciencedirect.com/science/article/pii/S2214860420306400.
17. The Virtual Foundry. *The Virtual Foundry - SDS - Copper 24-01*. 2024 [cited 2024 23 May]; Available from: https://thevirtualfoundry.com/wp-content/uploads/2024/03/The-Virtual-Foundry-SDS-Copper-24-01.pdf.
18. The Virtual Foundry. *Filawarmer, Strengthens Brittle Filament*. 2024 [cited 31 May 2024]; Available from: https://shop.thevirtualfoundry.com/en-za/products/filawarmer?variant=12228959993939.

19. Foundry, V. *PRINTING PURE METAL WITH FILAMET™*. 2023 [cited 2023 23 April]; Available from: https://thevirtualfoundry.com/help/.
20. Foundry, V. *Sintering Carbon (0.5kg)*. 2023 [cited 2023 23 April]; Available from: https://shop.thevirtualfoundry.com/en-za/products/sintering-carbon-0-5kg-1?variant=31189805924435.
21. Merck. *Copper*. n.d. [cited 2024 23 May]; Available from: https://www.merckmillipore.com/ZA/en/product/Copper,MDA_CHEM-102703.
22. Polyfluor Plastics. *PLA Filament*. 2011 [cited 2024 2 June]; Available from: https://www.polyfluor.nl/assets/files/datasheet-pla-filament-uk.pdf.
23. BIPM, et al., *Evaluation of measurement data — Guide to the expression of uncertainty in measurement*. First ed. JCGM 100:2008 GUM 1995 with minor corrections. 2008.
24. Struers. n.d. [cited 2024 20 September]; Available from: https://www.struers.com/en/Products/Hardness-testing/Hardness-testing-equipment/Duramin-40#references.
25. Mitutoyo. *PORTABLE SURFACE ROUGHNESS TESTER SURFTEST SJ-210 SERIES*. n.d. [cited 2024 16 September]; Available from: https://www.mitutoyo.com/webfoo/wp-content/uploads/Surftest_SJ210.pdf.
26. The Virtual Foundry. *What's Needed to Get Printing*. 2023 [cited 2024 3 June]; Available from: https://thevirtualfoundry.com/getting-started-with-filamet/.
27. The Virtual Foundry. *The Virtual Foundry TDS Copper*. 2024 [cited 2024 16 September]; Available from: https://thevirtualfoundry.com/wp-content/uploads/2024/05/The-Virtual-Foundry-TDS-Copper-24-05-2.pdf.
28. Xometry.pro. *Selecting Right Surface Roughness for CNC Machining*. 2023 [cited 2024 27 June]; Available from: https://xometry.pro/en/articles/cnc-machining-surface-roughness/.
29. Ali, B.M. *An Experimental Study of Heat Transfer in Pool Boiling to Investigate the Effect of Surface Roughness on Critical Heat Flux*. 2024 [cited 2024 20 September]; Available from: https://doi.org/10.3390/chemengineering8020044.